Supplementary Information

Table of Contents

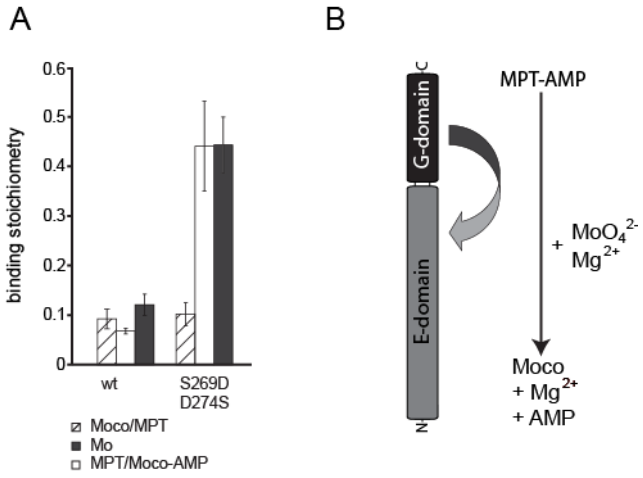

Supplementary Figure 1: Biochemical characterization of Cnx1E variant S269D D274S. (A) Quantitative detection of molybdenum cofactor (Moco)/molybdopterin (MPT), adenylated MPT (MPT-AMP), adenylated Moco (Moco-AMP) and molybdenum co-purified with the Cnx1E variant S269D D274S and wild type Cnx1E, respectively. Three full replicates were analyzed from which the HPLC fluorescence traces of biological replicate 2, technical replicate 1 are shown in supplementary Figure 2. The error bars shown correspond to the standard error of the mean. (B) Cnx1 domains and functionality. The C-terminal Cnx1G-domain catalyzes the formation of MPT-AMP which is subsequently transferred onto the N-terminal Cnx1E-domain. MPT-AMP is the substrate of Cnx1E and is converted to Moco in a Mg2+ and molybdate dependent manner[1].

A

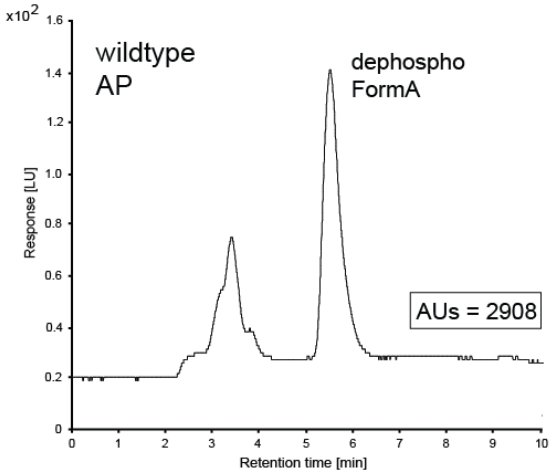
x10^2
wildtype
AP
dephospho
FormA
AUs = 2908
Response [LU]
Retention time [min]

B

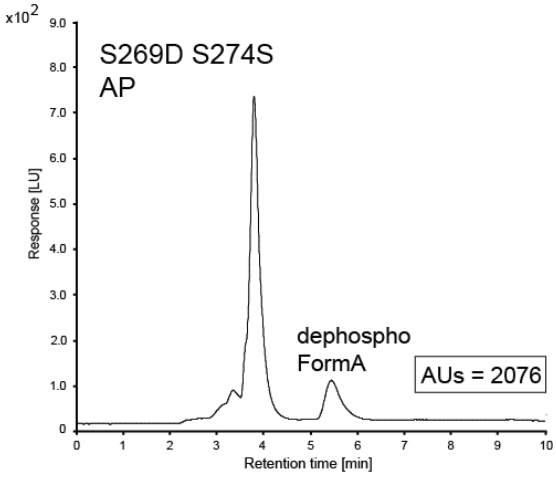
x10^2
S269D S274S
AP
dephospho
FormA
AUs = 2076
Response [LU]
Retention time [min]

C

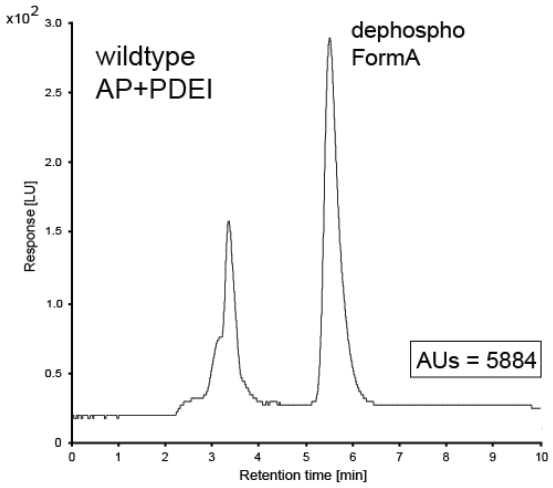
x10^2
wildtype
AP+PDEI
dephospho
FormA
AUs = 5884
Response [LU]
Retention time [min]

D

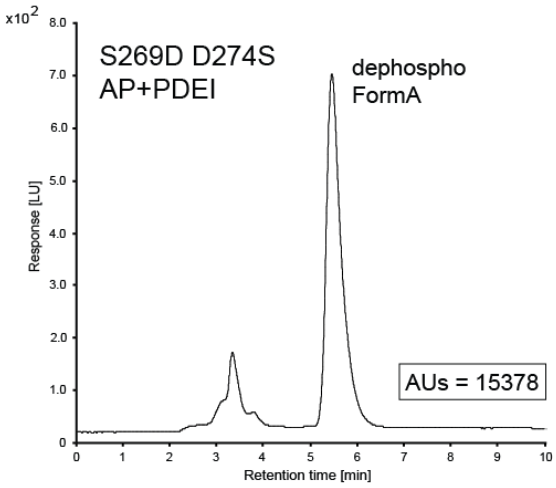
x10^2
S269D D274S
AP+PDEI
dephospho
FormA
AUs = 15378
Response [LU]
Retention time [min]

E

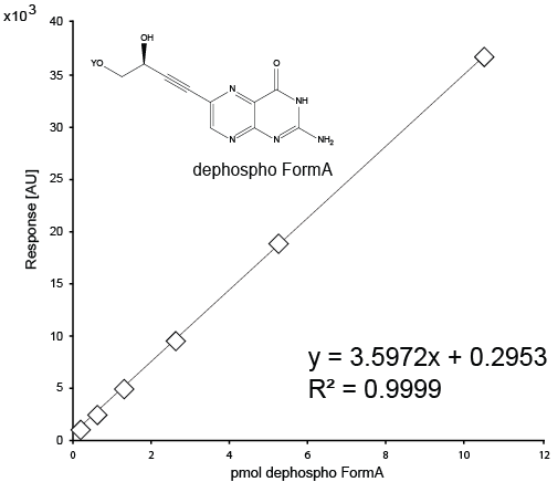
x10^-3
dephospho FormA
Response [AU]
y = 3.5972x + 0.2953
R² = 0.9999
pmol dephospho FormA

F

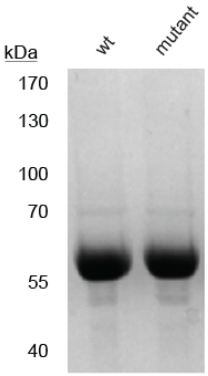
kDa
wt
mutant
170
130
100
70
55
40

Supplementary Figure 2: HPLC fluorescence traces derived from Cnx1E bound Moco/MPT and Moco/MPT-AMP. (A) - (D) HPLC fluorescence traces derived from Moco/MPT and Moco/MPT-AMP bound to wildtype (wt) Cnx1E and to variant S269D D274S. The results from the peak integrations are given as insets. The amount of protein bound Moco/MPT was detected as dephospho FormA upon treatment of the sample with alkaline phosphatase (AP)[2]. The amount of both, protein bound Moco/MPT and Moco/MPT-AMP was quantified as dephospho FormA upon the combined treatment of the sample with phosphodiesterase I (PDEI)[2] and alkaline phosphatase. For HPLC based FormA analysis, the following Cnx1E amounts were used: (A) 9.52 pmol Cnx1E wt, (B) 7.39 pmol Cnx1E variant S269D D274S, (C) 9.39 pmol Cnx1E wt, (D) 7.29 pmol Cnx1E variant S269D D274S. Shown are the results for biological replicate 2, technical replicate 1 (see supplementary Figure 1). (E) Dephospho FormA calibration curve using synthetic dephospho FormA[2,3]. The chemical structure of FormA is shown as inset (Y = PO_3H^-). For dephospho FormA Y = H[3]. Calculation of Moco/MPT and Moco/MPT-AMP occupancies was carried out as described in reference[2]. (F) 10 µg quantity of recombinant wildtype Cnx1E (biological replicate 2) and recombinant Cnx1E variant S269D D274S (mutant, biological replicate 2) were loaded onto a PA-gel, which was subjected to Coomassie blue staining after SDS–PAGE electrophoresis. The protein concentration of pure recombinant Cnx1E preparations used for ICP-MS based molybdenum quantification, HPLC based FormA quantification (see supplementary Figure 1) and PA-gel based purity control was determined using the Bradford assay (Roti-Quant; Roth) and bovine serum albumin as a concentration standard[4].

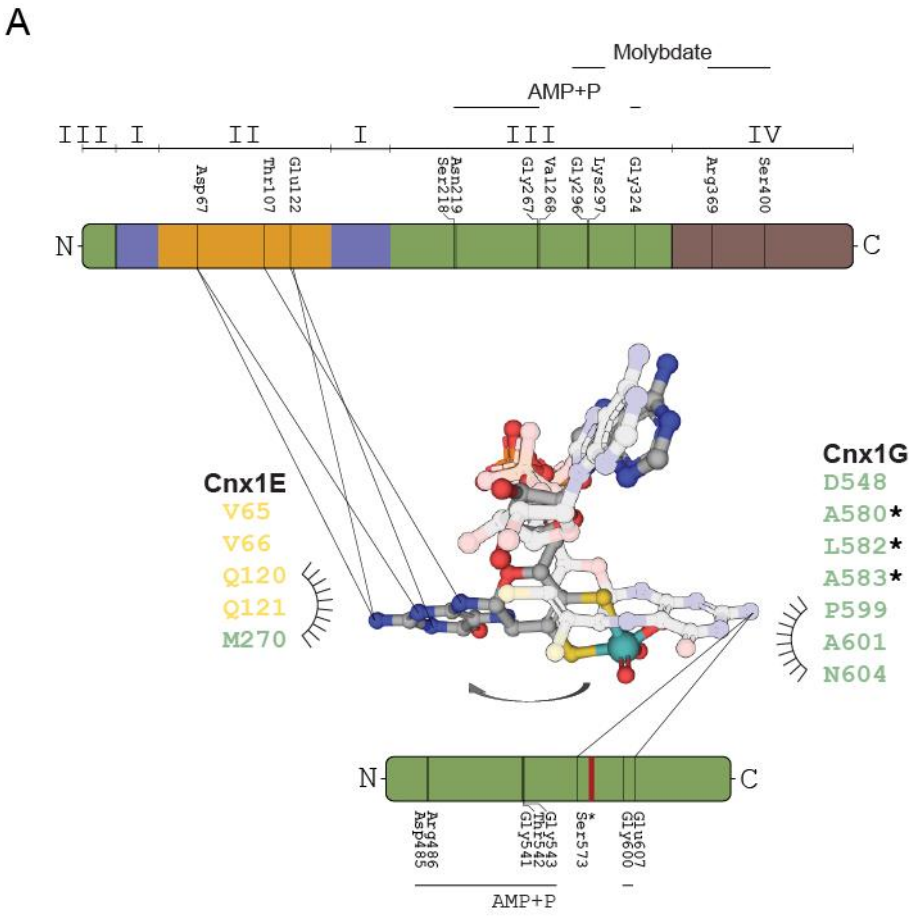
A
Molybdate
AMP+P
III I II I III IV
Asp67
Thr107
Glu122
Asn219
Ser218
Gly267
Val268
Gly296
Lys297
Gly324
Arg369
Ser400
N
C
Cnx1E
V65
V66
Q120
Q121
M270
Cnx1G
D548
A580*
L582*
A583*
P599
A601
N604
N
C
Arg486
Asp485
Gly543
Thr542
Gly541
*
Ser573
Glu607
Gly600
AMP+P

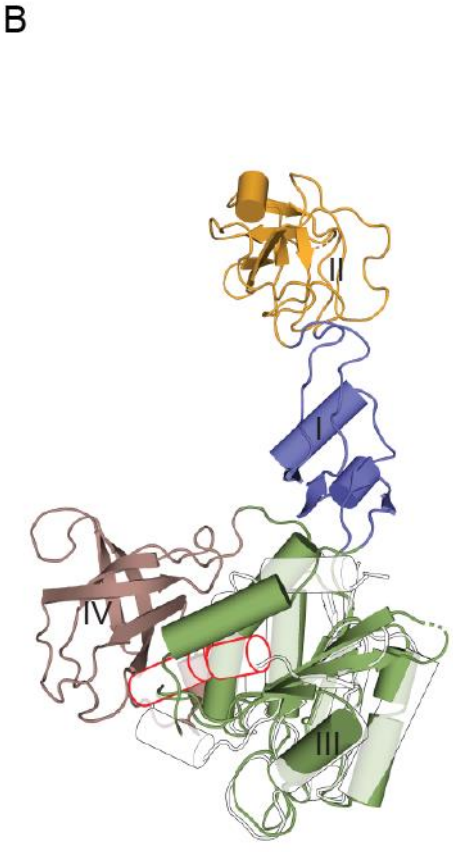
B
II
I
IV
III

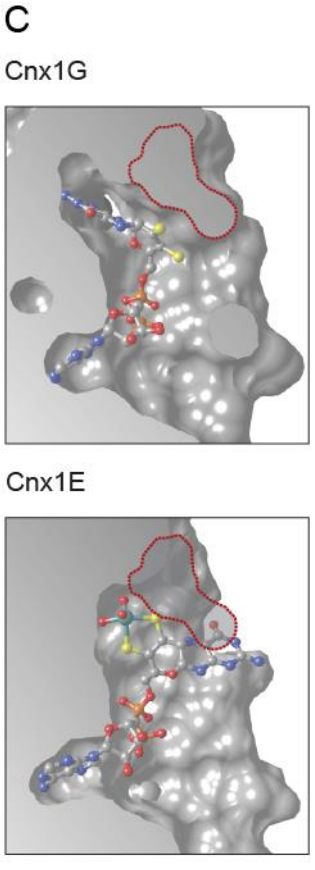
C
Cnx1G
Cnx1E

Supplementary Figure 3: Comparison of the Cnx1G and Cnx1E MPT/Moco-AMP binding properties. (A) Upper part: Schematic representation of Cnx1E subdomains. Individual subdomains (I to IV) are colored as in Figure 2. All amino acid residues involved in directed interactions with bound Moco-AMP are indicated (please see Supplementary Figure 4 for comparison). Direct interactions between subdomain II amino acids and the Moco moiety from Moco-AMP are indicated by solid lines. Hydrophobic interactions between Cnx1E residues with the Moco moiety of Moco-AMP are indicated next to the Moco-AMP / MPT-AMP superimposition derived from the superimposition of Cnx1G and Cnx1E (see figure part B). Color coding refers to subdomain II (yellow-orange) and subdomain III (forest-green) respectively. MPT-AMP is shown transparent, an arrow is indicating the movement, the MPT-AMP pterin part undergoes when transferred from Cnx1G to Cnx1E, the color code is the same as used in Figure 2. Lower part: Schematic representation of Cnx1G. Cnx1G is colored in forest-green. All amino acid residues involved in direct interactions with bound MPT-AMP are indicated[5]. Direct interactions between amino acid residues and the MPT moiety of MPT-AMP are depicted using solid lines. Hydrophobic interactions between Cnx1G residues with the MPT moiety of MPT-AMP are indicated next to the Moco-AMP / MPT-AMP superimposition. Asterisks indicate amino acids which were found to be part of a helix missing in the Cnx1G homologous Cnx1E subdomain III (please see figure part B). The position of this helix within Cnx1G is schematically shown as red box. (B) Superimposition of Cnx1G variant S583A[5] (PDB:1UUY) with Cnx1E variant S269D D274S (this study, PDB:6Q32). Cnx1E is colored as in Figure 2. The superimposed Cnx1G structure is shown outlined. Cnx1G matches to Cnx1E subdomain III, the RMSD value calculated is 1.44 Å. For clarity, bound MPT-AMP (Cnx1G) and Moco-AMP (Cnx1E) are not shown. The helix comprising amino acids 562-584 in Cnx1G that is absent in Cnx1E is outlined red. (C) Comparison of Cnx1G variant S583A (1UUY[5]) and Cnx1E (S269D D274S, PDB:6Q32) pterin-AMP binding sites. An intersecting plane of the binding sites is shown. The proteins are shown in colony-surface representation and in grey. Ligands are shown in ball and stick representation. The color code applied is the same as used in Figure 2. That part of $helix_{562-584}$ that prevents the MPT moiety of MPT-AMP from adopting a different conformation is framed in red. This frame has been superimposed on the Cnx1E active site where a corresponding helix is missing.

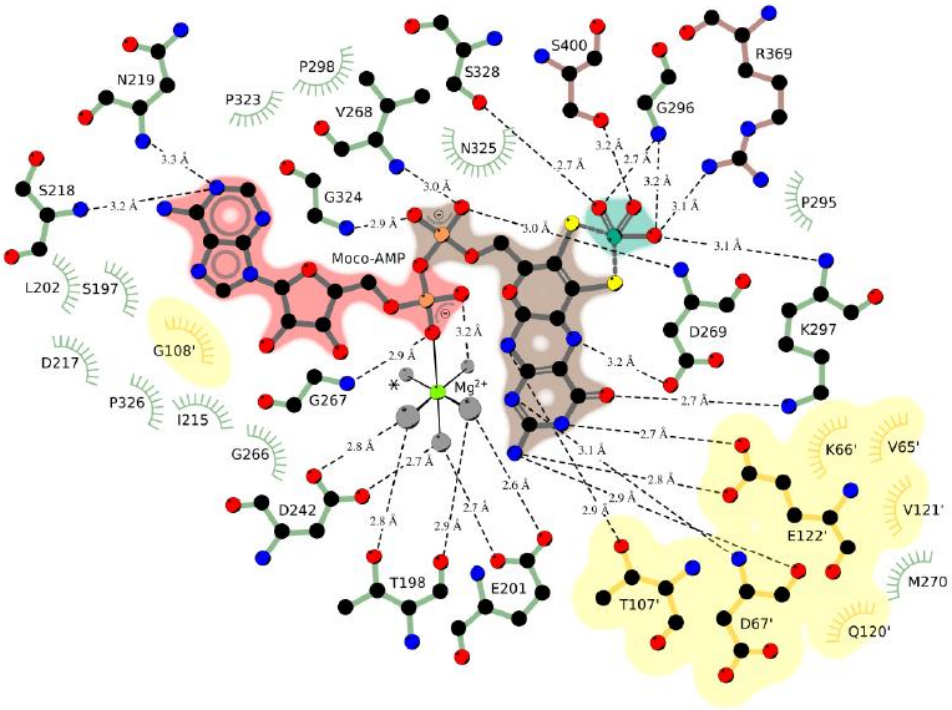

Supplementary Figure 4: Protein-ligand interactions in the active site of Cnx1E variant S269D D274S. Schematic representation of the protein-ligand interactions in the active site. Direct interactions are shown as broken lines with distances given in Angstroms. Amino acids involved in hydrophobic interactions are shown as coronas. The color of an amino acid indicates the corresponding subdomain of Cnx1E (see Figure 2). Amino acids highlighted by a yellow background belong to Cnx1E subdomain II. The AMP moiety of Moco-AMP is accentuated by a red, the MPT moiety by a brown, and the molybdate moiety by a teal background. The colors used in this figure are: slate-blue, subdomain I; yellow-orange, subdomain II; forest green, subdomain III; dark salmon, subdomain IV. Atoms are colored as described for Figure 2 with the exception of water molecules in the magnesium-water complex which are shown in gray and carbon atoms which are shown in black.

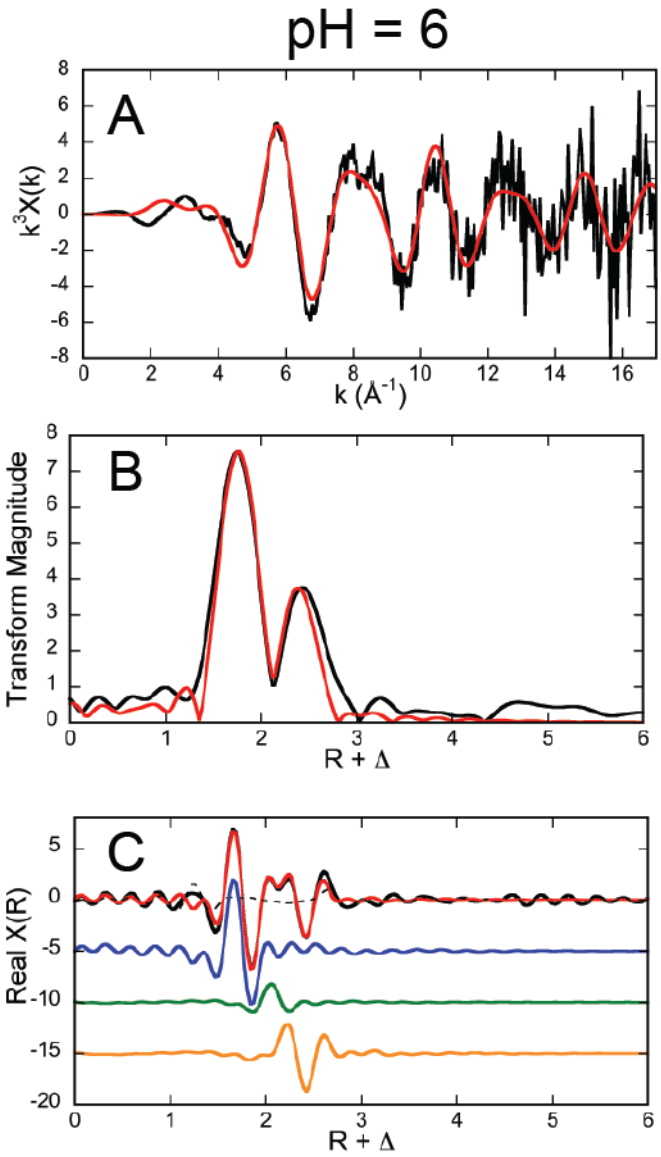

Supplementary Figure 5: Mo K-edge EXAFS data for Cnx1E variant S269D D274S at pH = 6. (A) EXAFS oscillations in k-space; (B) Fourier transforms of the EXAFS data presented in panel A; (C) The real part of the Fourier transform. The data is presented as black lines and the best fits to the data are depicted in red. The blue, green and orange colored lines in Panel C are the individual contributions from the oxo, OH, and S scattering paths, respectively. The Fourier transformed data have been phase-corrected using Mo-oxo backscattering. The highest bond length resolution (ΔR) expected from EXAFS data is defined by $\Delta R \geq \pi/2\Delta k$[6]. Therefore, given the range of our k-space data we should ideally be able to resolve bond length differences that are greater than ~ 0.17 Å. This resolution allows one to distinguish between Mo-oxo, Mo-thiolate, and Mo-hydroxide/water ligands.

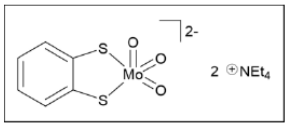
2-
S
O
Mo
O
O
S
2 ⊕NEt4

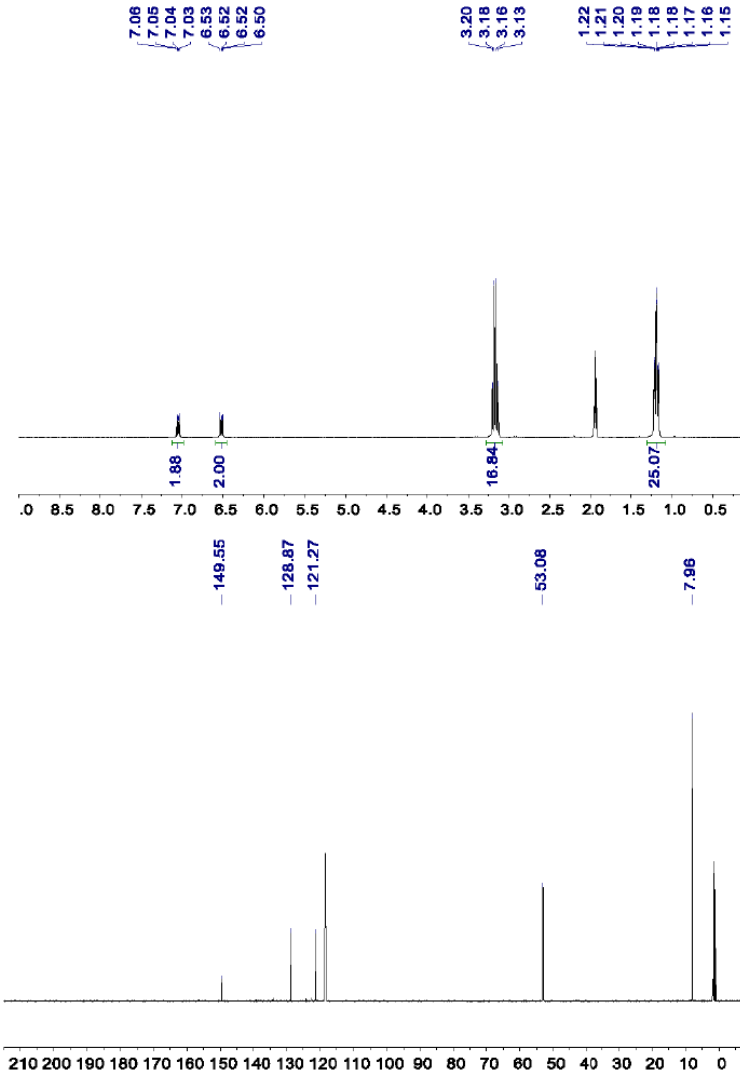
7.06
7.05
7.04
7.03
6.53
6.52
6.52
6.50
3.20
3.18
3.16
3.13
1.22
1.21
1.20
1.19
1.18
1.18
1.17
1.16
1.15
1.88
2.00
16.84
25.07
149.55
128.87
121.27
53.08
7.96

Supplementary Figure 6: ^{1}H (300 MHz) (top) and ^{13}C (125 MHz) (bottom) NMR spectra of model compound 2 in CD_3CN: (2) The synthetic procedure followed methods detailed in[7]. A solution of $[MoO_4](NEt_4)_2$ (500 mg, 1.19 x 10^{-3} mol, 1 eq) in dry acetonitrile (15 mL) was cooled to -10 °C in an ice / salt bath. To this solution was added an acetonitrile (5 mL) solution of 1,2-$C_6H_4(SSiMe_3)_2$ (341 mg, 1.19 x 10^{-3} mol, 1 eq). The resulting mixture was stirred at -10 °C for 5 minutes during which time, the solution gradually became orange. Dry *N,N*-dimethylacetamide (2 mL) was added to the reaction mixture by syringe. The reaction was kept at -10 °C, while the solution was concentrated under vacuum. Solids began to appear. The reaction was placed under nitrogen, and dry THF (80 mL) was added to the flask by syringe. More solids formed. The mixture was filtered through a glass frit. The solids were collected, washed with dry Et_2O, and dried under vacuum. Yield: 496 mg, 9.11 x 10^{-4} mol, 77 %. ATR-IR: 878, 825, 810 cm^{-1}.

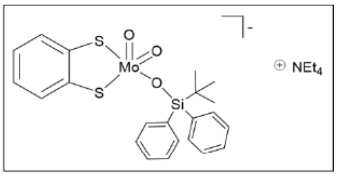
S
O
Mo
O
S
O
Si
NEt4

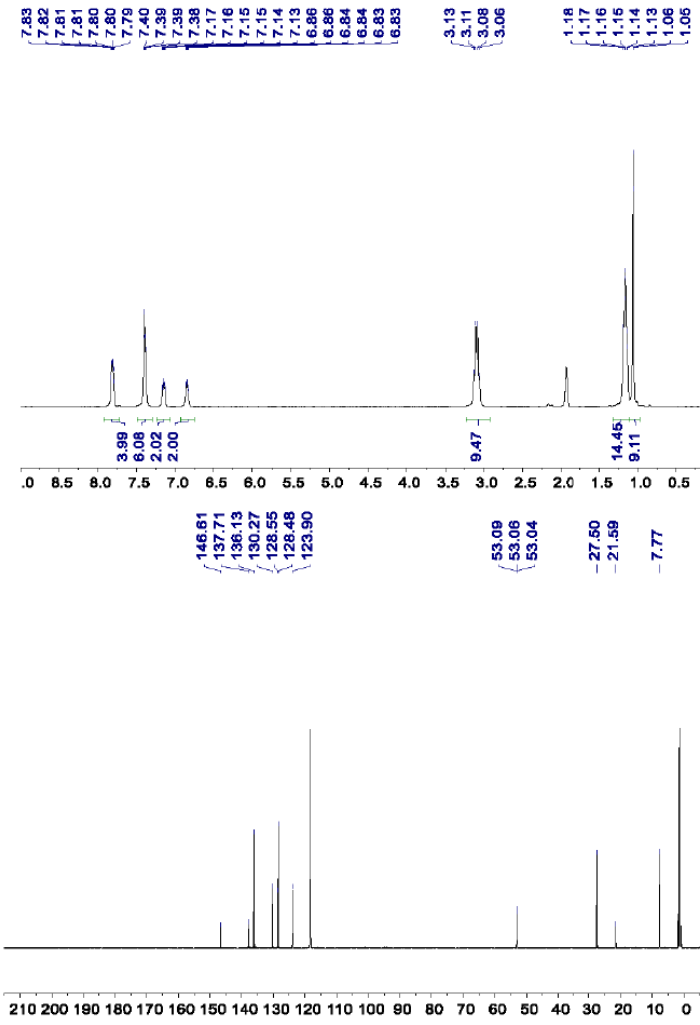
7.83
7.82
7.81
7.81
7.80
7.80
7.79
7.40
7.39
7.39
7.38
7.17
7.16
7.15
7.15
7.14
7.13
6.86
6.86
6.84
6.84
6.83
6.83
3.13
3.11
3.08
3.06
1.18
1.17
1.16
1.15
1.14
1.13
1.06
1.05
3.99
8.08
2.02
2.00
9.47
14.45
9.11
.0 8.5 8.0 7.5 7.0 6.5 6.0 5.5 5.0 4.5 4.0 3.5 3.0 2.5 2.0 1.5 1.0 0.5 0
146.61
137.71
136.13
130.27
128.55
128.48
123.90
53.09
53.06
53.04
27.50
21.59
7.77
210 200 190 180 170 160 150 140 130 120 110 100 90 80 70 60 50 40 30 20 10 0 -10

Supplementary Figure 7: ^{1}H (500 MHz) (top) and ^{13}C (125 MHz) (bottom) NMR spectra of model compound 3 in CD_3CN: (3) The synthetic procedure followed methods detailed in[8]. Solid $[MoO_3(OSiBu^tPh_2)](NEt_4)$ (2 g, 3.78 x 10^{-3} mol, 1 eq) was added to a solution of 1,2-benzenedithiol (H_2bdt, 650 mg, 4.57 x 10^{-3} mol, 1.2 eq) in acetonitrile (30 mL). The resulting orange solution was stirred at room temperature for 30 minutes before the solvent was removed under vacuum. The residual brown solid was washed with Et_2O (3 x 30 mL) and then dried under vacuum. Yield: 1.91 g, 2.92 x 10^{-3} mol, 77 %. ^{1}H NMR (CD_3CN, 300 MHz): δ 7.88 – 7.70 (m, 4H), 7.46-7.32 (m, 6H), 7.21 – 7.07 (m, 2H), 6.93 – 6.72 (m, 2H), 3.09 (q, *J* = 7.3 Hz, 8H), 1.15 (td, *J* = 6.9, 3.4 Hz, 12H), 1.05 (s, 9H). ^{13}C NMR (CD_3CN, 125 MHz): δ 146.61, 137.71, 136.13, 130.27, 128. 55, 128.48, 123.90, 53.06, 27.50, 21.59, 7.77. ATR-IR: 1481, 1441, 1424, 1391, 1362, 1235, 1173, 1107, 1000, 959, 940, 910, 876, 822, 783, 702, 691, 666, 623, 614, 537, 504, 489, 437 cm^{-1}.

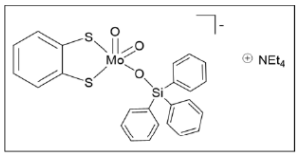
S
O
Mo
O
S
O
Si
NEt4

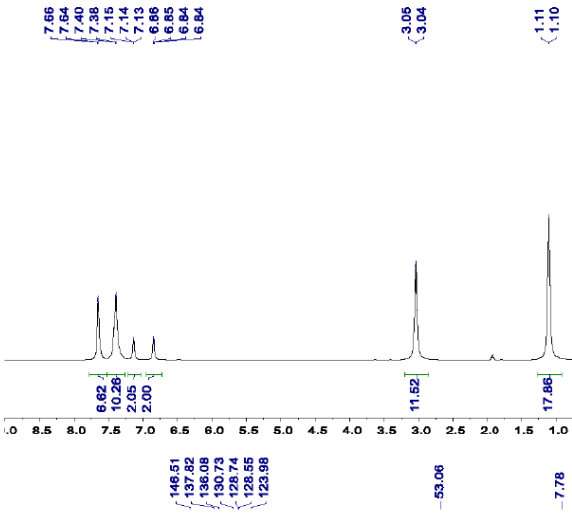
7.66
7.64
7.40
7.38
7.15
7.14
7.13
6.86
6.85
6.84
6.84
3.05
3.04
1.11
1.10
6.62
10.28
2.05
2.00
11.52
17.86
8.5 8.0 7.5 7.0 6.5 6.0 5.5 5.0 4.5 4.0 3.5 3.0 2.5 2.0 1.5 1.0 0.5 0
146.51
137.82
136.08
130.73
128.74
128.55
123.98
53.06
7.78
210 200 190 180 170 160 150 140 130 120 110 100 90 80 70 60 50 40 30 20 10 0 -10

Supplementary Figure 8: ^{1}H (500 MHz) (top) and ^{13}C (125 MHz) (bottom) NMR spectra of model compound 4 in CD_3CN: [(bdt)MoO_2($OSiPh_3$)](NEt_4). (4) The synthetic procedure followed the methods detailed in[9]. $MoO_2(OSiPh_3)_2$. (881 mg, 1.30 x 10^{-3} mol, 1 eq), dilithio-1,2-benzenedithiolate (Li_2bdt, 200 mg, 1.30 x 10^{-3} mol, 1 eq), and NEt_4Cl (430 mg, 2.60 x 10^{-3} mol, 2 eq) were added, as solids, to a 100 mL Schlenk flask equipped with a magnetic stir bar. Freshly distilled THF (50 mL) was added to the Schlenk flask by syringe, and the resulting reddish-orange solution was stirred at room temperature for approximately 30 minutes. A brown solid formed. The crude reaction mixture was filtered through Celite. The reddish-orange filtrate was collected and concentrated under vacuum, and the concentrated solution was triturated with dry Et_2O (100 mL). An orange-tan solid formed. The solid was removed by filtration and dried under vacuum. Yield: 216 mg, 4.15 x 10^{-4} mol, 32 %. ^{1}H NMR (CD_3CN, 500 MHz): δ 7.78-7.53 (m, 6H), 7.52-7.26 (m, 9H), 7.20 – 7.07 (m, 2H), 6.92 – 6.77 (m, 2H), 3.04 (q, J = 7.3 Hz 8H), 1.10 (t, J = 7.3 Hz 12H). ^{13}C NMR (CD_3CN, 125 MHz): δ 146.51, 137.82, 136.08, 130.73, 128.74, 128.55, 123.98, 53.06, 7.78. ATR-IR: 1479, 1442, 1427, 1389, 1171, 1113, 999, 958, 912, 882, 783, 740, 703, 507 cm^{-1}. (4a) The synthetic procedure followed methods detailed in[9]. To a solution of $MoO_2(OSiPh_3)_2$ (500 mg, 7.37 x 10^{-4} mol, 1 eq) in THF (25 mL) was added a THF (5 mL) solution of dilithio-1,2-benzenedithiolate (Li_2bdt, 125 mg, 8.11 x 10^{-4} mol, 1.1 eq). The reaction was stirred at room temperature for 30 minutes. During this time, the reaction solution changed colors from dark blue to dark orange. The reaction mixture was treated with a slurry of PPh_4Cl (607 mg, 1.62 x 10^{-3} mol, 2.2 eq) in THF (10 mL) and stirred at room temperature of another hour. The dark orange solution was filtered through Celite. The collected solids were washed with additional THF (3 x 10 mL) and the solvent was removed from the collected filtrates to yield an orange solid. Yield: 187 mg, 2.12 x 10^{-4} mol, 29 %. Crystals were grown by vapor diffusion of Et_2O into a THF solution of [(bdt)MoO_2($OSiPh_3$)](PPh_4). ^{1}H NMR (CD_3CN, 300 MHz): δ 7.94 – 7.85 (m, 6H), 7.78 – 7.67 (m, 12H), 7.67-7.59 (m, 8H), 7.43 – 7.30 (m, 9H), 7.09 (ddd, J = 5.8, 3.3, 0.9 Hz, 2H), 6.80 (ddd, J = 5.8, 3.4, 0.9 Hz, 2H). ^{13}C NMR (CD_3CN,125 MHz): δ 146.56, 137.91, 136.41 (d, JC-P = 3.3 Hz), 136.12, 135.71 (d, JC-P = 10.2 Hz), 131.37 (d, JC-P = 12.8 Hz), 130.67, 128.72, 128.48, 123.85, 118.92 (d, JC-P = 89.2 Hz). ATR-IR: 1482, 1438, 1427, 1391, 1106, 999, 954, 910, 880, 743, 722, 703, 687, 664, 613, 525, 504 cm^{-1}.

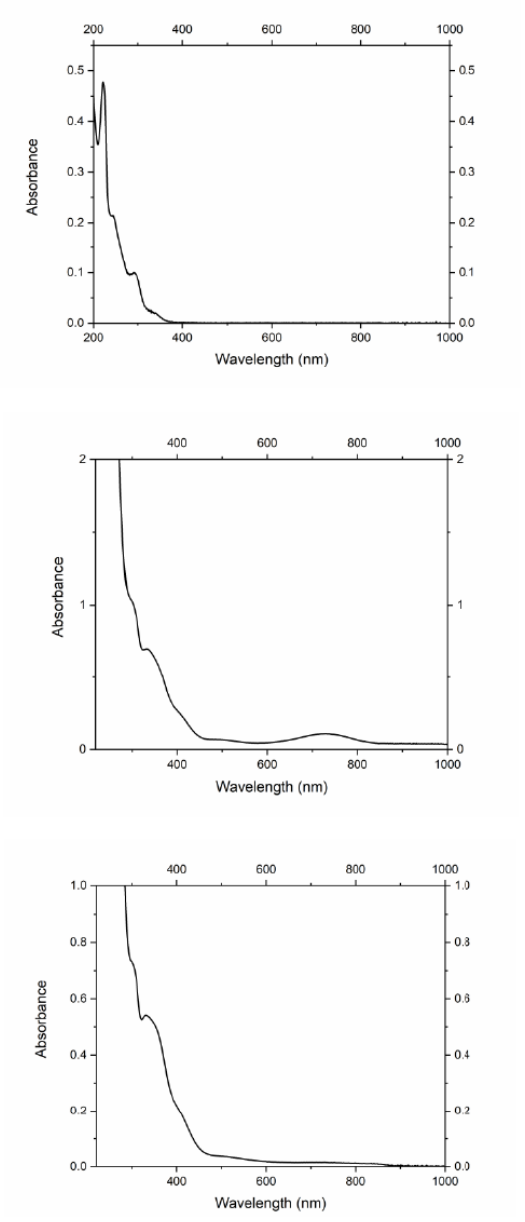

Supplementary Figure 9: 300 K (room temperature) electronic absorption spectra of 2 (top), 3 (middle), and 4 (bottom) in MeCN.

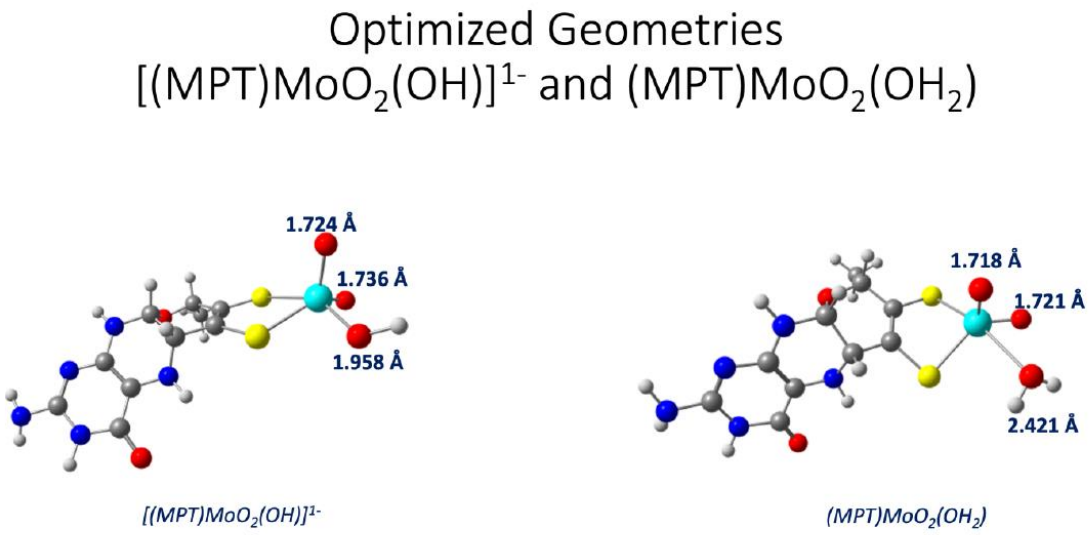

Supplementary Figure 10: Optimized geometries of $[(MPT)MoO_2(OH)]^{1-}$ and $(MPT)MoO_2(OH_2)$. Note the markedly longer Mo-O(aqua) bond in $(MPT)MoO_2(OH_2)$ compared to the Mo-O(hydroxide) bond in $[(MPT)MoO_2(OH)]^{1-}$. The computational details are given in the Materials and Methods section.

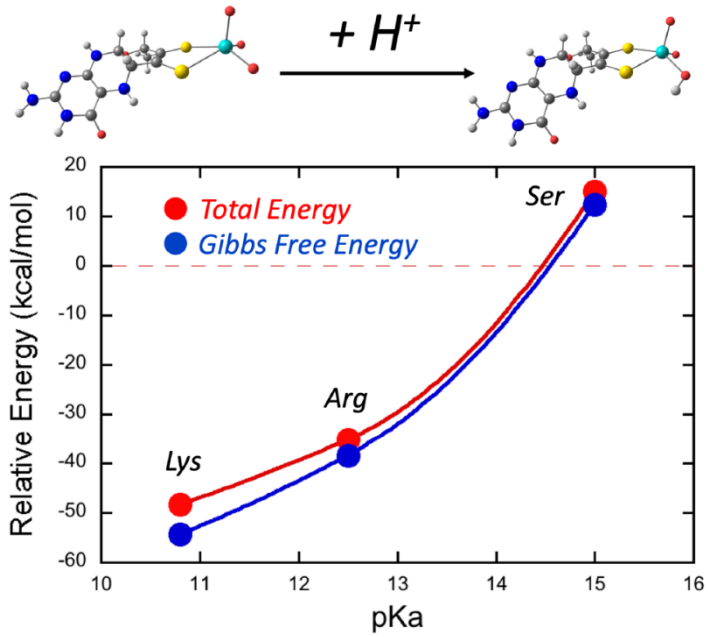

Supplementary Figure 11: Computed total energies and Gibbs free energies as a function of amino acid side chain pKa values. Note that the pKa's of Lys and Arg are such that they represent the most likely candidates for protonating $[(MPT)MoO_3]^{2-}$ to yield $[(MPT)MoO_2(OH)]^{1-}$. The computational details are given in the Materials and Methods section.

Supplementary Table 1: X-ray crystallographic data collection and refinement statistics. Numbers in parentheses account for the shell of highest resolution. [a]Effective (d_{eff}) and corresponding optical (d_{opt}) resolution of the dataset determined with EFRESOL[10]. [b]Data completeness for a volume in reciprocal space bounded by an ellipsoid centered on [000] and with the dimensions a = $1/d_{h00,min}$, b= $1/d_{0k0,min}$, c = $1/d_{00l,min}$. *statistics assuming Friedel's law be false.

	Cnx1E-S269DD274S	
Data collection		
Wavelength (Å)	0.9998	1.7462
Space group	I222	
Unit cell parameters		
a (Å)	65.01	
b (Å)	123.29	
c (Å)	133.14	
α≡β≡γ (°)	90	
Resolution (Å)		
$d_{hkl,max}$ – $d_{hkl,min}$	90.46 – 1.39 (1.49 – 1.39)	90.56 – 2.06 (2.11 – 2.06)
$d_{h00,eff}$	1.41	--
$d_{0k0,eff}$	1.79	--
$d_{00l,eff}$	1.41	--
$d_{eff,mean}$[a] [d_{opt}]	1.51 [~1.4]	2.06 [~1.8]
No. of reflections		
total	1,062,478 (48,205)	409,816 (12,879)
unique	80,156 (4,007)	33,113 (1,657)
Completeness		
spherical	0.746 (0.202)	0.987* (0.816)*
ellipsoidal[b]	0.961 (0.698)	--
Multiplicity	13.3 (12.0)	6.5* (4.1)*
Mean *I/σ(I)*	24.1 (1.3)	13.2 (5.2)
Wilson B (Å^2)	19.9	23.3
R_{merge}	0.056 (2.121)	0.141 (0.273)
R_{meas}	0.058 (2.215)	0.153 (0.315)
R_{pim}	0.016 (0.627)	0.058 (0.153)
CC1/2	0.999 (0.445)	0.979 (0.939)
No. of reflections used	80,112 (4,005)	
R_{work} / R_{free}	0.1596 / 0.1762	
No. of non-hydrogen atoms		
total	3,657	
in protein	3,149	
in ligands	73	
in ordered solvent	435	
Atomic B-factors (Å^2)		
Average	28.2	
Protein/Ligands/Solvent	27.1 / 23.5 / 37.6	
No. of amino acid residues		
total / ordered	470 / 420	
RMSD from ideal		
bonds (Å)	0.014	
angles (°)	1.71	
Ramachandran (%)		
favored	98.79	
allowed	0.97	
outliers	0.24	

Supplementary Table 2: Dihedral angles ζ and η of MCD and bis-MGD structures that are deposited in the Protein Data Bank.

Mo-enzyme family	Structure	Dihedral ζ (°)	Dihedral η (°)
DMSO-Reductase*	1aa6	99.75	68.25
		82.91	*108.84*
	1dmr	-156.48	-63.99
		-171.60	*-46.93*
	1e18	-155.69	-61.92
		-173.19	*-41.09*
	1e5v	-162.67	-58.05
		-163.37	*-51.52*
	1e60	-157.68	-66.30
		-169.81	*-50.76*
	1e61	-155.43	-68.26
		-178.18	*-39.02*
	1eu1	-165.75	-52.73
		-166.86	*-52.60*
		-152.61	-70.80
		-159.98	*-63.92*
	1fdi	147.62	63.01
		100.47	*92.76*
	1fdo	140.75	70.32
		113.20	*82.27*
	1g8j	-133.96	-50.81
		-119.81	*-47.87*
	1g8k	-133.94	-54.28
		-127.45	*-44.78*
	1h0h	-174.48	-83.09
		-175.45	*-6.95*
	1h5n	-156.93	-62.61
		-174.20	*-40.33*
		-155.68	-64.58
		-179.08	*-35.14*
	1kqf	-122.98	-69.50
		-124.88	*-60.54*
	1kqg	-139.91	-47.11
		-132.53	*-44.28*
	1ogy	170.10	-2.34
		-167.26	*-22.97*
	1r27	145.10	-22.27
		94.10	*54.98*
	2dmr	-153.76	-77.55
		-168.33	*-59.75*
	2e7z	98.22	55.13
		125.77	*77.74*
		128.68	*72.22*
	2iv2	-140.39	-91.40
		89.85	*105.20*
	2jim	-150.36	-40.72
		-131.50	*-42.23*
	2jio	-142.60	-33.40
		-129.93	*-39.49*
	2jip	-139.71	-44.13
		-122.28	*-53.46*
	2jiq	-139.45	-44.55
		-146.54	*-26.83*
	2jir	-153.81	-34.05
		-124.00	*-44.64*
	2nap	-146.92	-37.72
		-140.29	*-48.79*
	2nya	-139.73	-52.62
		-97.50	*-67.57*
	2v3v	-140.78	-42.61
		-128.90	*-38.62*
	2v45	-131.28	-42.37
		-119.56	*-58.73*

2vpw	175.99	-23.70
	156.08	*-83.81*
2vpx	175.98	-23.30
	155.93	*-83.70*
2vpy	175.95	-23.53
	156.05	*-83.87*
2vpz	176.02	-23.42
	156.01	*-83.87*
3dmr	-159.16	-59.49
	179.58	*-34.84*
3egw	116.13	60.41
	102.02	*62.10*
3ml1	-145.50	-49.59
	-111.21	*-57.35*
3o5a	-145.26	-50.01
	-108.28	*-60.98*
4aay	-137.45	-56.41
	-133.43	*-45.95*
4dmr	-150.95	-69.05
	-168.47	*-49.55*
4ydd	74.73	99.42
	66.36	*103.79*
5ch7	61.01	103.79
	105.02	*62.54*
	68.22	101.14
	99.01	*64.82*
	69.55	108.14
	100.87	*62.91*
5chc	55.64	110.75
	105.94	*59.47*
	61.51	107.92
	104.32	*59.92*
	74.75	106.19
	110.76	*53.10*
5e7o	78.47	101.23
	73.80	*92.30*
	73.28	98.59
	118.70	*45.41*
	68.74	99.52
	101.09	*60.54*
	73.07	103.52
	80.08	*83.14*
	86.46	94.40
	111.89	*50.25*
	79.66	102.22
	116.74	*40.82*
5nqd	-140.95	-49.58
	-130.59	*-41.42*
	-146.97	-43.45
	-128.62	*-43.50*
	-136.06	-46.92
	-120.74	*-58.37*
5t5i	-178.44	-25.52
	117.30	*74.48*
	179.14	-26.32
	121.85	*69.21*
5t5m	179.02	-22.37
	128.07	*68.21*
6cz7	89.85	84.30
	1.83	*152.39*
	88.59	81.28
	5.83	*149.29*

	6cz8	82.40	87.62
		1.24	*156.20*
		84.04	88.16
		4.69	*150.81*
	6cz9	94.50	77.99
		5.62	*150.00*
		89.30	80.56
		4.17	*151.01*
	6cza	83.91	88.19
		5.85	*149.53*
		85.66	82.97
		5.65	*149.95*
Xanthine dehydrogenase	1dgj	-143.26	66.80
	1ffv	-152.88	65.90
		-152.67	64.38
	1n5w	-158.91	65.00
		-155.25	63.43
	1n60	-152.93	62.08
		-157.47	67.01
	1n61	-154.93	61.50
		-158.71	66.63
	1n62	-154.08	63.18
		-156.28	65.45
	1n63	-155.83	63.66
		-157.31	63.67
	1rm6	-159.38	81.47
		-159.99	80.37
	1sb3	-158.55	82.12
		-158.01	80.75
	1sij	-158.30	75.42
	1t3q	-125.71	75.89
		-132.72	73.85
	1vlb	-159.64	79.42
	1zxi	-154.61	64.27
		-155.57	63.77
	3fc4	-158.40	82.11
	3hrd	-134.65	64.28
		-139.30	64.13
	3l4p	-158.55	81.40
	4czy	-157.24	80.52
	4czz	-158.54	82.61
	4c80	-157.18	80.88
	4us8	-159.16	82.98
	4us9	-157.83	81.22
	4usa	-158.66	81.49
	4zoh	-156.30	87.06
	5g5g	-154.43	82.42
	5g5h	-145.51	64.84
	5y6q	158.64	107.51
Cnx1G	1uuy	-141.34	-170.89
Cnx1E	6q32 (this work)	-75.06	150.89

Supplementary Table 3: EXAFS Data Best Fit Results for Cnx1E S269D D274S at pH 6 and pH 8. 2a and 3a are the bond lengths from crystal structures of model compounds [(bdt)Mo(VI)O_3]$(NEt_4)_2$ (2) and [(bdt)Mo(VI)O_2(OSitBuPh$_2$)](NEt_4) (3). a: fits in the first and second rows use the crystal structure of 3. 5b details of the bond lengths from the TDDFT optimized geometry of [(MPT)Mo(VI)O_2(OH)]$^{1-}$ using the B3LYP functional and mixed basis set (6-31g* for light atoms and LANL2DZ for Mo atom with LANL2 ECP). Solvation effect was taken into account and used water as solvent but adopting eps=4 for mimicking the protein environment. b: fits in the third and fourth rows adopt the optimized structure with [(MPT)Mo(VI)O_2(OH)]$^{1-}$. For each back-scattering path, N is the coordination number; R is the interatomic distance in Å; σ^2 is the mean-square deviation of the interatomic distance with unit of Å^2. ΔE_0 is the energy shift relative to the threshold E_0 in eV. The weighted R factor gives the fractional misfit and is defined as sqrt[$\Sigma k^6(X_{exp}$- Xfit)$^2/\Sigma k^6 X^2_{exp}$].

Enzyme/Model	Mo-Oxo			Mo-O			Mo-S			ΔE_0	R_f (%)
	N	R	σ^2	N	R	σ^2	N	R	σ^2		
[a]Insertase pH6	2	1.741(6)	0.0017(1)	1	2.114(8)	0.0032(6)	2	2.466(2)	0.0057(9)	-7.981(8)	13.29
[a]Insertase pH8	2	1.764(2)	0.0022(1)	1	2.029(9)	0.0082(1)	2	2.484(3)	0.0074(3)	-4.033(7)	12.48
[b]Insertase pH6	2	1.743(3)	0.0018(2)	1	2.116(5)	0.0042(1)	2	2.472(5)	0.0060(3)	-6.385(2)	12.76
[b]Insertase pH8	2	1.766(4)	0.0023(5)	1	2.032(8)	0.0071(3)	2	2.485(5)	0.0074(6)	-2.861(6)	8.67
2[a] (crystal)	3	1.748					2	2.545			
3[a] (crystal)	2	1.711		1	1.911		2	2.460			
5[b] (opt)	2	1.730		1	1.959		2	2.485			

Supplementary Table 4: EXAFS fitting parameters for Cnx1E variant S269D D274S at pH 6.

Fits	Mo-Oxo			Mo-O			Mo-S			ΔE_0	R_f (%)
	N	R	σ^2	N	R	σ^2	N	R	σ^2		
Fit 1	2	1.743	0.0018	1	2.116	0.0042	2	2.472	0.0060	-6.385	12.76
Fit 2	4	1.753	0.0066				2	2.466	0.0065	0.945	41.13
Fit 3	3	1.756	0.0042				2	2.478	0.0066	3.158	21.77
Fit 4	2	1.756	0.0014				2	2.489	0.0062	-0.541	15.45

Supplementary Table 5: EXAFS fitting parameters for Cnx1E variant S269D D274S at pH 8.

Fits	Mo-Oxo			Mo-O			Mo-S			ΔE_0	R_f (%)
	N	R	σ^2	N	R	σ^2	N	R	σ^2		
Fit 1	2	1.766	0.0023	1	2.032	0.0071	2	2.485	0.0075	-2.861	8.67
Fit 2	4	1.758	0.0083				2	2.456	0.0073	-8.327	51.52
Fit 3	3	1.758	0.0055				2	2.465	0.0074	-6.579	32.53
Fit 4	2	1.759	0.0024				2	2.477	0.0070	-4.019	14.68

References

1 Llamas, A., Otte, T., Multhaup, G., Mendel, R. R. & Schwarz, G. The Mechanism of nucleotide-assisted molybdenum insertion into molybdopterin. A novel route toward metal cofactor assembly. *J Biol Chem* **281**, 18343-18350, doi:10.1074/jbc.M601415200 (2006).

2 Hercher, T. W. *et al.* Insights into the Cnx1E catalyzed MPT-AMP hydrolysis. *Biosci Rep* **40**, doi:10.1042/BSR20191806 (2020).

3 Klewe, A., Kruse, T. & Lindel, T. Aminopyrazine Pathway to the Moco Metabolite Dephospho Form A. *Chemistry* **23**, 11230-11233, doi:10.1002/chem.201702274 (2017).

4 Krausze, J. *et al.* Dimerization of the plant molybdenum insertase Cnx1E is required for synthesis of the molybdenum cofactor. *Biochem J* **474**, 163-178, doi:10.1042/BCJ20160846 (2017).

5 Kuper, J., Llamas, A., Hecht, H. J., Mendel, R. R. & Schwarz, G. Structure of the molybdopterin-bound Cnx1G domain links molybdenum and copper metabolism. *Nature* **430**, 803-806, doi:10.1038/nature02681 (2004).

6 Graham N. George, R. M. G., Roger C. Prince, K. V. Rajagopalan. The Molybdenum Site of Sulfite Oxidase: A Comparison of Wild-Type and the Cysteine 207 to Serine Mutant Using X-ray Absorption Spectroscopy. *J. Am. Chem. Soc.* **118**, 8588-8592 (1996).

7 Partyka, D. V. & Holm, R. H. Oxygen/sulfur substitution reactions of tetraoxometalates effected by electrophilic carbon and silicon reagents. *Inorg Chem* **43**, 8609-8616, doi:10.1021/ic040097g (2004).

8 Wang, J. J. & Holm, R. H. Silylation, sulfidation, and benzene-1,2-dithiolate complexation reactions of oxo- and oxosulfidomolybdates(VI) and -tungstates(VI). *Inorg Chem* **46**, 11156-11164, doi:10.1021/ic701294y (2007).

9 Lim, B. S., Willer, M. W., Miao, M. & Holm, R. H. Monodithiolene molybdenum(V, VI) complexes: a structural analogue of the oxidized active site of the sulfite oxidase enzyme family. *J Am Chem Soc* **123**, 8343-8349, doi:10.1021/ja010786g (2001).

10 Urzhumtseva, L. & Urzhumtsev, A. EFRESOL: effective resolution of a diffraction data set. *Journal of Applied Crystallography* **48**, 589–597 (2015).